Journal of
Nanoscience and Nanotechnology
Vol. 11, 3899–3910, 2011

RESEARCH ARTICLE

Template Assisted Electrochemical Growth of Cobalt Nanowires: Influence of Deposition Conditions on Structural, Optical and Magnetic Properties

Andrea Cortés[1], Roberto Lavín[2, 3], Juliano C. Denardin[3], Ricardo E. Marotti[4], Enrique A. Dalchiele[4], Patricio Valdivia[5], and Humberto Gómez[6, *]

[1] *Departamento de Física, Universidad Técnica Federico Santa María, Casilla 110-V, Valparaíso, Chile*
[2] *Facultad de Ingeniería, Universidad Diego Portales, Ejército 441, Santiago, Chile*
[3] *Departamento de Física, Universidad de Santiago de Chile, Av. Ecuador 3493, Santiago, Chile*
[4] *Instituto de Física, Facultad de Ingeniería, Herrera y Reissig 565, C.C. 30, 11000 Montevideo, Uruguay*
[5] *Agricultural and Biosystems Engineering Department, University of Arizona, Tucson, AZ 85721-0038, USA*
[6] *Instituto de Química, Facultad de Ciencias, Pontificia Universidad Católica de Valparaíso, Casilla 4059, Valparaíso, Chile*

The influence of electrodeposition potential, pH, composition and temperature of the electrolytic bath on the structure of cobalt nanowires arrays electrodeposited into anodic aluminum oxide (AAO) porous membranes is reported. XRD, SEM, and TEM analysis were employed to characterize structural (crystal phase, crystallographic texture, and grain size), and morphological nanowire properties. It was confirmed that at pH 2 the electrodeposition potential has not influence on the preferred crystallographic orientation of the electrochemically grown Co nanowires. At pH 4 the electrodeposition potential controls the growth of cobalt nanowires along some preferential crystallographic planes. The electrolytic pH bath modulates the fcc or hcp phase exhibited by the cobalt nanowires. Single crystalline nanowires with a hcp phase strongly oriented along the (20$\bar{2}$1) crystallographic plane were obtained at pH 4 and at −1.1 V (vs. Ag/AgCl), a result not previously reported. High electrolytic bath temperatures contributed to improve the single crystalline character of the cobalt nanowires. The presence of chloride anion in the electrolytic bath also influenced on the structural properties of the resulting cobalt nanowires, improving their crystallinity. The optical reflectance of the samples shows a structure in the UV-blue region that can be assigned to the two-dimensional morphology arising in the shape of the almost parallel nanowires. Magnetic measurements showed that different electrodeposition potentials and electrolytic bath pH lead to different magnetic anisotropies on the nanowire array samples.

Keywords: Cobalt, Nanowires, Electrodeposition, Magnetic Properties.

1. INTRODUCTION

In the last years, fabrication of nanowire arrays, principally magnetic nanowires, has become the subject of intensive study and research.[1–6] Magnetic nanowires have attracted attention because their distinctive properties are of great interest in theoretical physics and solid-state science.[1–6] Their potential applications in high-density magnetic recording devices,[1–6] giant magnetoresistance[7] and spintronics are also of high interest.[8, 9] For instance, magnetic nanowire arrays as high-density magnetic storage material can achieve recording densities of more than 100 Gbit/in,[2] which is beyond the projected thermal limit of 40 Gbit/in^2 for continuous magnetic films.[10, 11]

Cobalt (Co) is an important ferromagnetic material with large coercivity and high Curie temperature (1400 K) that has two kinds of phases: Hexagonal close-packed (hcp, α-Co) phase at low temperatures and face-centered cubic (fcc, β-Co) phase at high temperature, both presenting different properties.[8, 12] Furthermore, nanoscaled Co structures particularly often crystallize in the fcc β-Co phase.[13] Among the different magnetic nanowires (Fe, Co and Ni), Co has been focus of attention motivated by its large crystal anisotropy when the material is in the hcp structure.[14] Particular interest arise in cobalt nanowire (CoNW) arrays because Co is a hard magnetic material whose magnetic properties can be engineered through variation of the structural parameters, such as, crystallinity, shape, and grain size.[15]

*Author to whom correspondence should be addressed.

Different fabricating methods of one-dimensional nanowires have been explored in recent years. Among these, the template-based electrochemical method is widely used because it is simple, inexpensive technique, fast and operating at near room temperature.[2, 3, 16–19] In addition, the ability to "tailor-make" properties (i.e., preferred crystallographic orientation) by controlling deposition conditions, and uniform growth makes electrodeposition an attractive synthesis method.[20] Arrays of NWs are obtained by electrochemically filling a porous template that contains a large number of straight cylindrical holes with a controllable narrow size distribution. The filling of the pores is gradually produced from the bottom to the template surface, and the amount of material can be easily controlled through the charge recorded during the nanowires growth. This makes possible the preparation of highly ordered nanostructures with specific dimensions and properties.[2, 3, 16–19] Two types of templates have been mainly used: porous anodic aluminum oxide (AAO) and etched ion track polycarbonate membranes.[21] AAO template, which possesses a uniform and parallel hexagonal porous structure,[22–23] is widely used as template for the assembling of high-quality nanowire arrays. An advantage of the AAO membranes is the possibility to control their morphological features by adjusting the anodizing parameters, i.e.,: surface treatment of aluminum, potential and time of anodizing, nature and composition of electrolyte.[22, 24, 25] A variety of metallic NWs such as Fe,[26] Ni,[27, 28] Cu,[28–30] Ag,[28, 31, 32] and Au[28, 33] have been fabricated in a single bath using a template-based electrochemical method. Furthermore, Co nanowires have been electrodeposited into the porous of AAO templates by DC,[15, 34, 35] AC,[36, 37] multistep AC[38] and pulsed potential methods.[12, 39] However, the dependence of their crystal structures with the experimental conditions is still controversial.[37]

Given that it has been demonstrated that the nanowires (NWs) properties depend strongly on the crystallographic orientation,[12] controlling the growth orientation is essential for many of their proposed applications. As the magnetic property of bulk Co differs greatly along the different crystalline orientations,[34] one feasible route to control the magnetic properties of Co NWs is to modulate the crystallographic orientation. Although some groups tried to control the orientation of Co nanowires, it is still a considerable challenge to do it rationally. Moreover, the NWs structure needs to be precisely controlled because the magnetic properties are also structure related.

The interest in Co NW immersed in a dielectric matrix is not only reduced to its magnetic and magneto-optic properties,[40] but also to its optical properties. The optical properties of metal-dielectric composite materials, with cobalt as the corresponding metal, have been recently studied in detail for cobalt spherical and elongated nanoparticles.[41–43] In the past, Co-Al_2O_3 composite were studied for their application as solar selective surface in photothermal energy conversion of solar energy.[44] More recently, the interest has grown because of its potential application of their surface plasmon renonances,[43, 45] which in conjunction with the magnetic properties can lead to versatile hybrid magneto-optic and optoelectronic devices. The study of the surface plasmon resonance of Co NW[46] and their non-linear optical properties[47] were studied in suspension in liquid solutions. For Co NW arrays in Al_2O_3 the optical properties were studied in the infrared region.[48]

The current paper reports the growth of Co NW arrays with controllable orientation and phase structure by potentiostatic electrodeposition into AAO templates. The influence of electrodeposition potential, electrolytic bath acidity, bath temperature and the presence of chloride anion in the electrolytic bath on the crystal phase, crystallographic texture, and grain size of the resulting Co NWs have been studied and reported. Also, the optical properties in the visible and near UV region of Co NWs inside the alumina template are studied and interpreted using an effective medium numerical approach. Finally, the influence of electrodeposition conditions (electrodeposition potential and electrolytic bath pH) in the magnetic behavior of the samples (associated with the influence of these parameters in the mechanism of nanowire growth) is also discussed.

2. EXPERIMENTAL DETAILS

Anodic aluminum oxide (AAO) membranes were prepared from a 99.99% aluminum foil (0.13 mm thickness, SIGMA-ALDRICH) by the two-step anodization technique as described in a previous paper.[32] To facilitate the electric contact, a very thin Au-Pd layer was sputtered on one side of the membrane followed by the electrodeposition of a thicker cobalt layer for achieving the full pore sealing.

The electrochemical experiments were performed with an IM6e BAS-ZAHNER potentiostat controlled through a PC. The electrochemical cell consisted in a three electrode arrangement with the AAO/Co layer as working electrode, a platinum foil as counter-electrode, and Ag/AgCl(sat) as reference. All the potentials in the text are referred to this reference electrode. The cobalt nanowires were deposited under potentiostatic control at room temperature in an unstirred electrolyte solution containing 0.4 M $CoSO_4$ and 0.28 M H_3BO_3 at pH = 2 and pH = 4, the pH was adjusted by adding H_2SO_4 or NaOH. To study the effect of chloride ions 0.4 M $CoSO_4$, 0.08 M $CoCl_2$ and 0.28 M H_3BO_3, pH 2 plating solution was used.

The morphological characterization of the AAO was made with an Atomic Force Microscope (AFM, Nanoscope IIIa, Digital Instrument, contact mode). X-ray diffraction analyses were conducted with a Philips PW3 710 diffractometer using the CuK_α radiation.

A JEOL 5900 LV apparatus was used for SEM measurements. Transmission electron microscopy (TEM) observations were carried out on a JEOL 2010F electron microscope operated at 200 kV coupled with an energy dispersive spectrometer Princeton Gamma Technology system. A 1 nm diameter probe was used for the microanalysis. Samples were prepared by crushing samples in an agate mortar and ultrasonically stirring them in butanol. The smallest particles were then collected in the supernatant liquid using a holey C-coated copper grid.

The optical properties of the samples were studied by diffuse reflectance spectroscopy. The experimental setup is similar to the one used for the optical characterization of other metallic nanowires in this template.[31] In the present case, however, the samples under studied were the metal-dielectric nanostructures consisting in the cobalt nanowires immersed in the template (nanoporous alumina). The light source consisted of a 1000 W electric power Xe lamp (ORIEL 6271). The unpolarized light output reached the sample after being chopped with an SRS SR540 chopper and monochromated with an ORIEL 77250 monochromator. The reflected light was detected normally to sample surface (with quasi-normal incidence) with an UDT 11-09-001-1 (100 mm^2 wide area UV enhanced unbiased silicon detector). A first lock-in amplifier (SRS SR530) extracted the signal from the detector while a second lock-in amplifier (EG&G 5209) was used to measure the variation of the optical source amplitude. A PC controlled the whole process (monochromator movement and GPIB communication with the lock-in). For the present study the Xe white light was used as reference for reflectance determination.

The magnetization measurements were performed in a VSM (vibrating sample magnetometer) and a SQUID (superconducting quantum interference device) at 300 K.

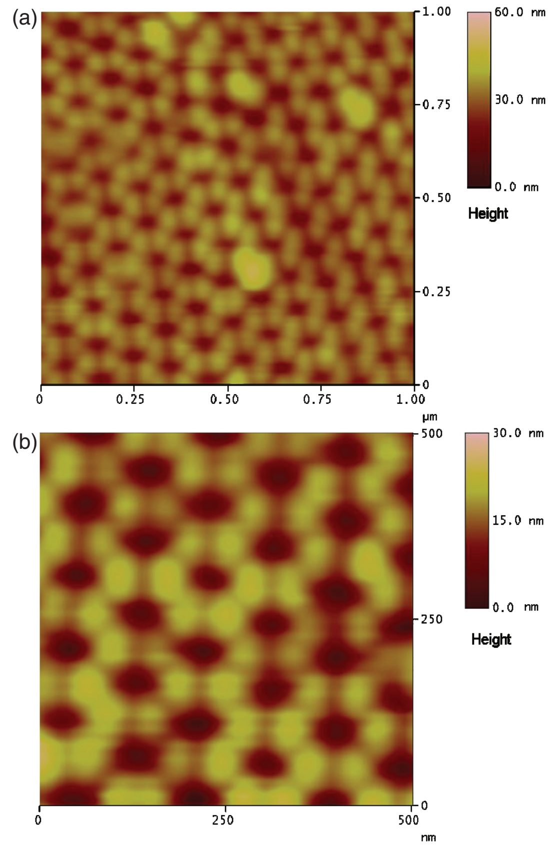

Fig. 1. AFM top view of a highly ordered home made AAO template at low- and high-magnification: (a) 1.00×1.00 μm^2, and (b) 500×500 nm^2.

3. RESULTS AND DISCUSSION

3.1. Morphological Study of the AAO Membrane Template and Co Nanowires

Figure 1 shows a top view AFM micrographs of the AAO template with the typical self-ordered cell configuration which was formed under the most appropriate conditions in oxalic acid solution at room temperature (20 °C). An almost ideal arranged hexagonal cell configuration is observed with monodomain size of up to several square micrometers (Fig. 2(a)), a pore density of 10^{10} pores/cm^2, an average pore's radius of of 25 nm, and an interpore spacing, D_{int}, of 100 nm.

The cross-sectional SEM view of the membrane in Figure 2(b), showed that the pores are cylindrical, open at one end, propagated through the entire thickness of the membrane ($\sim$6 μm). They are also straight, parallel perpendicular to the surface, and not connected to each other.

Figure 3, panels (a and b), are SEM images of Co NWs prepared on the home made AAO template with a pore diameter of 50 nm, after partial or total dissolution of the alumina membrane. The SEM observations show Co NWs with a high aspect ratio that are independent and parallel to each other, continuous, and densely packed. They exhibited an average length of 6 μm which is equivalent to the thickness of the AAO prepared membranes. Figure 4 shows typical Co NWs TEM images. The images reveal that the nanowires have a uniform diameter of about 50 nm, which is equal to the pore size of the AAO template.

3.2. Effect of the Electrodeposition Potential and Electrolyte pH Bath on the Structure of the Co Nanowire Arrays

The X-ray diffraction technique was used to investigate the crystallographic phase, the overall crystalline quality, and the possible texture of the cobalt nanowire (CoNW) arrays. Figure 5 shows typical X-ray diffraction scans for cobalt nanowire arrays embedded in the alumina template that were grown at different electrodeposition potentials at pH = 2, at room temperature. Irrespective of the electrodeposition potential, only a predominant single peak is observed at $2\theta = 75.9°$. This diffraction peak is difficult to index, because the Bragg reflection angle of $2\theta = 75.868°$

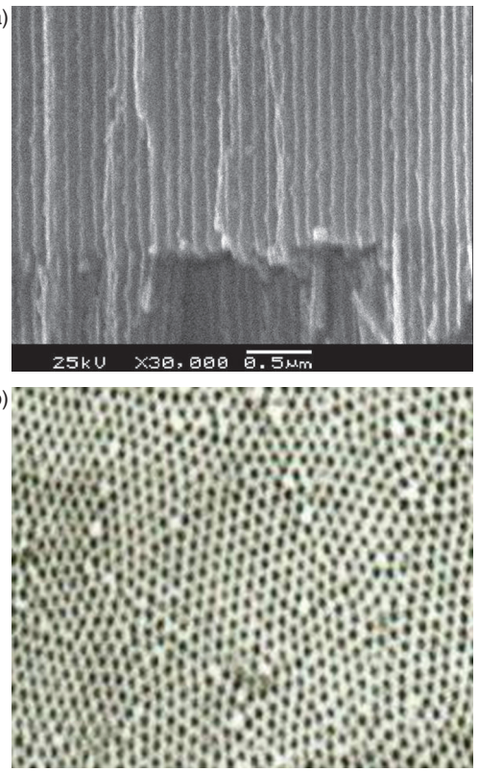

Fig. 2. SEM (a) top view and (b) cross section (×30.000) of a home made AAO template.

for Co fcc(220) lies close to that of 75.891° for Co hcp(11$\underline{2}$0) (JCPDS 89-4307 and JCPDS 89-4308, respectively). It should be noted that, in spite that at room temperature the stable phase for bulk Co is only hcp (see above), the fcc phase can also appear in nanostructures or very thin films.[13, 50, 51] Additionally, it has been reported that the bath pH significantly affects the structure of Co formed by elctrodeposition.[13, 50, 51] Actually, a solution with low pH (<2.5) favours fcc Co, whereas higher pH values (>2.5) favours the formation of hcp Co.[13, 50, 51] Therefore, current results are in line with the relevant literature involving low-dimensional CoNWs and low pH electrodeposition of Co. Based on previously reported work, it can be asserted that the single peak in Figure 5 originates either from pure fcc or a combination of the hcp and fcc phases.

The sharp and narrow diffraction peaks indicates that the nanowires have highly preferential orientation, not dependent on the electrodeposition potential. However, the relatively small signal/noise in the CoNW diffraction patterns reveals that they are not single crystals but rather consist of oriented polycrystals. The dimensions of the crystallites, of which the cobalt nanowires are composed, were estimated from the FWHM of the principal diffraction peaks using the Scherrer formula.[52] When the term "crystallite size" is used, we are referring to the dimensions of the coherent diffracting domain. The equation is applicable to samples where lattice strain is absent. Nanowires can posses some strains, which could also be a factor contributing to the peaks width, thereby affecting the estimation of the crystallite nanowires size. Moreover, the crystallite sizes of the cobalt nanowires estimated from the X-ray diffraction peak width (and using Scherrer's formula), were in some cases greater than 45 nm. Thus, crystallite sizes were larger than the maximum accurate size value acceptable that can be deduced from these XRD measurements. Therefore, the size of the crystalline domains determined from the XRD peak widths is used only as a comparative measure among samples. The crystallite sizes (along the nanowire axis) of Co nanowires grown at different electrodeposition potentials are presented as an inset in Figure 5(c). A marked increase in crystallinity is observed as the electrodeposition potential is made more cathodic. This behavior is consistent with previously published results for Ni[53–55] and Co[36] nanowires in which the growth of single-crystal nanowires under high deposition overpotential was observed. Moreover, a very good understanding of the single-crystal growth of Ni and CoNWs under high deposition overpotentials has been recently presented.[56] A higher deposition overpotential promotes a selective surface adsorption of H ions onto the intrinsic high-energy crystal face lowering its surface energy, even lower than that of the previously intrinsic low-energy crystal face. Consequently, the formation of the crystalline nucleus favors the growth of single-crystal nanowires along the normal direction of the intrinsic high-energy crystal face.[56]

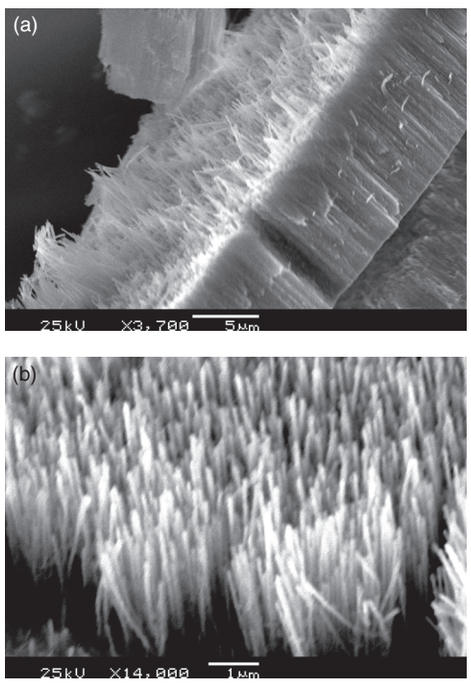

Fig. 3. SEM micrographs of the exposed Co nanowires after the alumina template membrane was partial or total dissolved away.

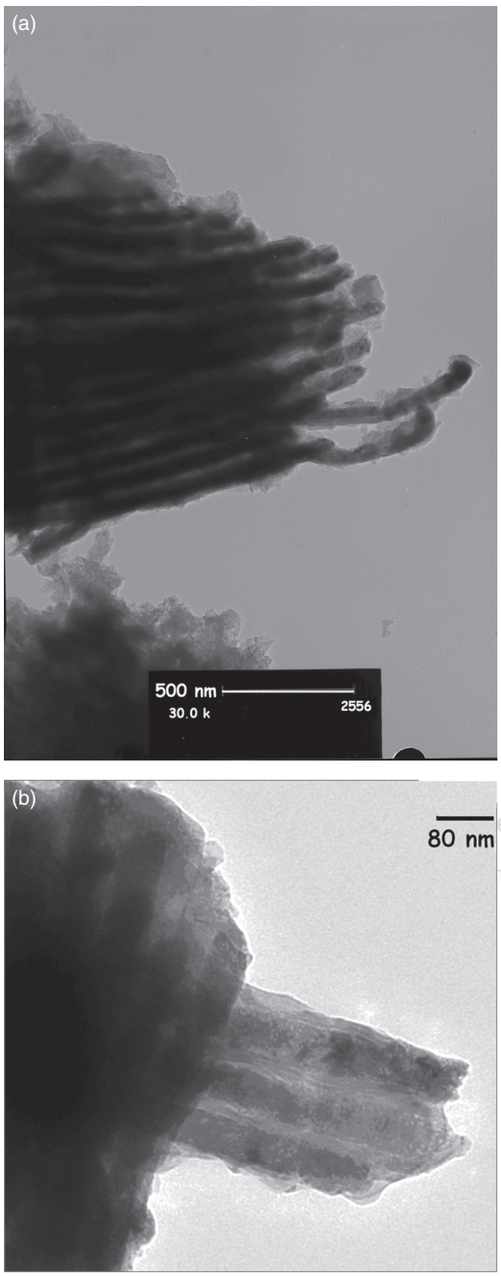

Fig. 4. TEM micrographs of cobalt nanowires that have been grown at −0.900 V, inside a 50 nm AAO template.

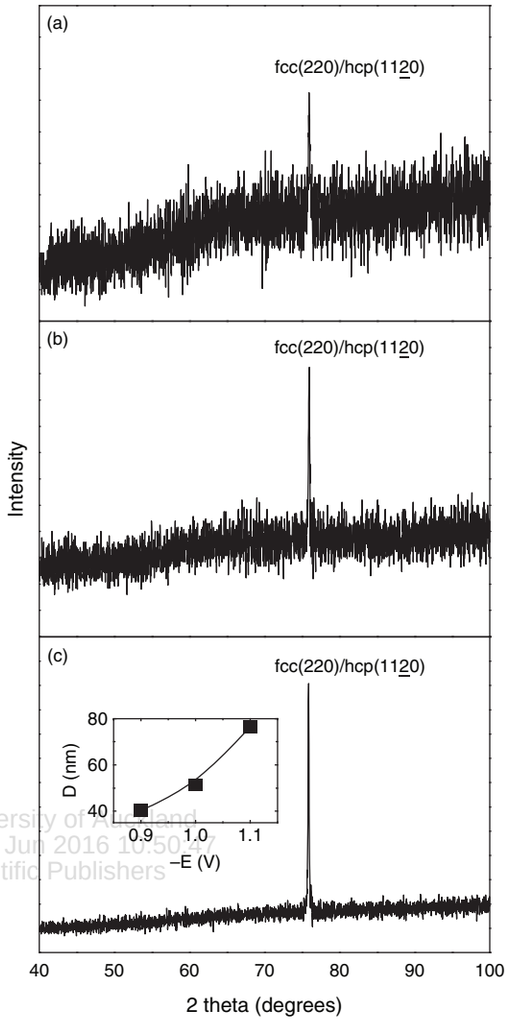

Fig. 5. X-ray diffraction patterns of cobalt nanowire arrays embedded in the home made AAO template. The cobalt nanowires have been grown at different electrodeposition potentials: (a) −0.9 V, (b) −1.0 V and (c) −1.1 V. Bath temperature: 20 °C, and pH = 2. Inset of Figure 3(c) shows a plot of the crystallite sizes (along the nanowire axis) of Co nanowires grown at different electrodeposition potentials.

Figure 6 displays the XRD patterns of CoNW arrays grown at pH = 4 at two electrodeposition potentials (−0.9 and −1.1 V), at room temperature. Figure 6(a) shows the X-ray diffractogram corresponding to CoNWs fabricated at −0.9 V. All the peaks can be indexed as the Co hcp phase. The intensity of the diffraction peak corresponding to hcp(10$\underline{1}$0) plane is very strong indicating that the c-axis is perpendicular to the CoNWs axis direction. The XRD pattern for the CoNW arrays grown at −1.1 V shown in Figure 6(b), exhibits only one predominant diffraction peak at $2\theta = 94.6°$, corresponding to (20$\underline{2}$1) plane of hcp Co. To the best of our knowledge, it is the first time that Co nanowires with a very strong hcp (20$\underline{2}$1) preferred crystallographic orientation, as in the present case, has been reported. Significant differences of crystal structures are observed between CoNW grown at pH = 2 (see Fig. 5) and those grown at pH = 4 (see Fig. 6), indicating that the crystal structure of CoNWs depends strongly on the pH value of the electrolytic bath. For pH 2.0 (Fig. 5), they crystallize in a mixture fcc and hcp structures. Instead, at pH 4.0 (Fig. 6), CoNWs crystallize in the hcp structure. This behavior is consistent with previously published results.[38]

During the electrodeposition of Co the hydrogen evolution reaction (HER) occurs as a side reaction. The

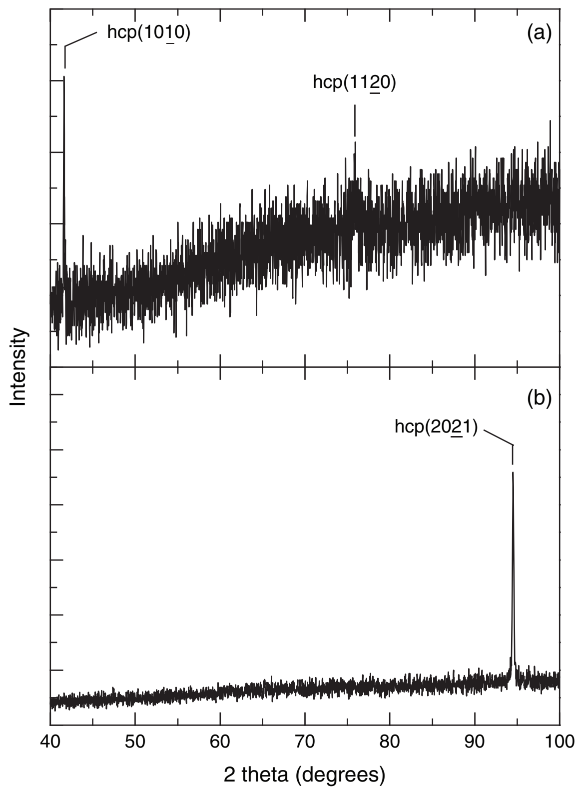

Fig. 6. X-ray diffraction patterns of cobalt nanowire arrays embedded in the home made AAO template. The cobalt nanowires have been grown at room temperature, in an electrolytic bath with pH = 4, and at two different electrodeposition potentials: (a) −0.9 V and (b) −1.1 V.

consequences are: a current efficiency reduction, a pH change at the interface and a modification in the kinetics Co ions electroreduction. According to Matsushima et al.[57] an hydrogen rich phase is formed during cobalt reduction (Eq. (1)). They assume that an electrochemical desorption and diffusion process of adsorbed hydrogen molecules from the electrode surface can be associated with the dissolution of hydrogen rich cobalt phase (Eqs. (2 and 3)) as:

$$H_3O^+ + e^- + Co \rightarrow CoH_{(ads)} + H_2O \quad (1)$$

$$H_3O^+ + CoH_{(ads)} + e^- \rightarrow H_{2,(ads)} + H_2O + Co \quad (2)$$

$$H_{2,(ads)} \rightarrow H_{2(g)} \quad (3)$$

This assumption agrees with our experiments because we observed bubbles formation over the electrode for deposits obtained at pH 2.

At pH 4.1, the same authors[57] detected the simultaneous deposition of Co and $Co(OH)_2$ (see Eq. (4)). They assumed that the formation rate of cobalt hydroxide in the vicinity of the electrode decreases and the remaining current is used in the direct discharge of Co^{2+} ions. The absence of hydroxide species can be related to the decreasing amount of free OH^- ions reacting with Co^{2+} in the vicinity of the electrode surface, leading to direct Co deposition (Eq. (5)),

$$Co^{2+}_{(aq)} + 2OH^-_{(aq)} \rightarrow Co(OH)_{2,(s)} \quad (4)$$

$$Co^{2+}_{(aq)} + 2e^- \rightarrow Co_{(s)} \quad (5)$$

Nakahara[51] suggested a mechanism for the formation of fcc cobalt at low pH, which is actually metastable cobalt hydride, promoted by the codeposition of atomic hydrogen. The formation of hcp Co probably occurs at higher pH (>3), where the current is largely used for the reduction of metals ions, although a delay in the reduction rate due to hydroxide adsorption can occurs.

3.3. Effect of Bath Temperature on the Structure of the Co Nanowire Arrays

Figure 7 shows the XRD patterns of CoNW arrays grown at −1.1V at two different electrolytic bath temperatures: 20 °C and 40 °C, pH = 2. Irrespective of the bath temperature, the presence of only one diffraction peak corresponding to the fcc(220)/hcp(11$\bar{2}$0) plane is observed. It must be concluded that for this high electrodeposition potential the bath temperature has no effect on the preferred crystallographic orientation of the CoNWs over this temperature range. However, the diffraction peaks of nanowires grown at the higher temperature are more intense and present a narrow full width at high maximum when compared with those corresponding to samples obtained at the

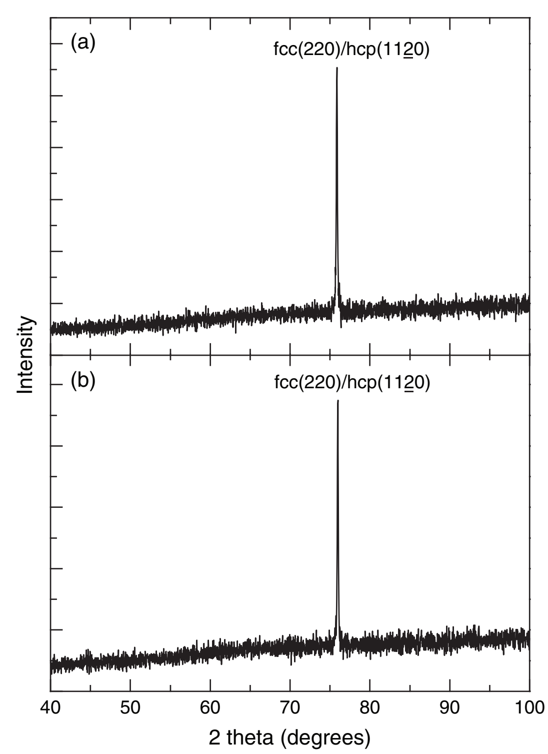

Fig. 7. X-ray diffractograms of home made AAO/Co nanowire arrays. The cobalt nanowires have been grown at −1.1 V, pH = 2; at two different bath temperatures: (a) 20 °C; and (b) 40 °C.

lower temperature, demonstrating a better crystalline structure and a superior single crystal quality. On the basis of Scherrer's equation, crystallite size values of 76 nm and 80 nm along the nanowire axis have been obtained for the CoNWs grown at 20 °C and 40 °C, respectively. Then, the increase of temperature benefits the crystalline structure of the CoNWs. Higher temperature promotes the surface diffusions of atoms and favors the re-growing and coalescence of pre-existing grains.

3.4. Effect of Chloride ion in the Electrolytic Bath on the Structural Properties of Co Nanowire Arrays

Figure 8 shows the XRD patterns of CoNW arrays that have been electrochemically grown at -1.1 V, pH $= 2$, at room temperature, in the absence (Fig. 8(a)), and in the presence of chloride ions (Fig. 8(b)) in the electrolytic bath. For both cases, only a predominant single peak is observable at $2\theta = 75.9°$, corresponding to Co fcc(220)/Co hcp(11$\underline{2}$0). On the other hand, crystallite size values obtained for CoNWs grown without and with the presence of chloride anions at 20 °C, are 76 nm and 84 nm along the fcc [110] direction, respectively. Therefore, the presence of chloride anion in the electrolytic bath also improves the crystallinity of the resulting CoNWs.

There are not references in the literature regarding the specific rol played by chloride ions on the cristallinity improvement of Co NW. However, some explanations have been given in the case of Co thin films electrodeposition. It is possible that something similar could happen with Co NW. It has been suggested that two-dimensional nucleation could change when hydrogen is simultaneously discharged and certain foreign additives are adsorbed on the cathode.[58, 59] It is known that Cl^- affects the metal deposition by specifically adsorbing on the cathode.[60] Furthermore, especially during electrodeposition of iron-group metals, it is also reported that an intermediate MOH^-_{ad} (M: Fe, Ni or Co) complex was formed during the reduction of simple hydrated iron-group metal ions and Cl^-, changing the structure of the intermediate to the more easily reducible MCl^-_{ad}. It is possible that these ionic species adsorbed on the cathode affected the nucleation and growth of the specific plane of the deposited Co.[58] However, in current work we have only studied one electrodeposition potential, therefore a wider potential interval need to be considered in order to validate these assumptions.

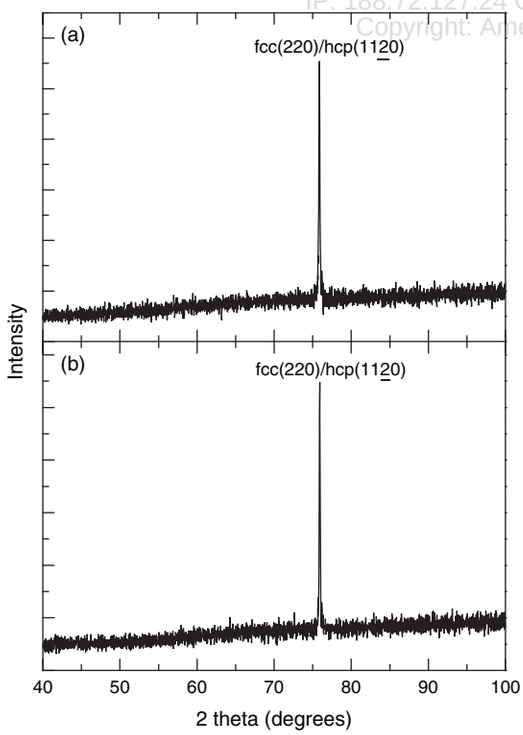

Fig. 8. X-ray diffractogram of home made AAO/Co nanowire arrays. The cobalt nanowires have been grown at -1.1 V, 20°C, pH $= 2$, in electrolytic baths: (a) In the absence, and (b) in the presence of chloride anion.

3.5. Optical Study

The metal-dielectric samples (Co nanowires immersed in the porous alumina) are dark black with a bluish hue in some samples. The dark color of moderately packed nanowires has been reported to arise in an enhanced absorption due to multireflection effect in the composite structure.[61, 62] Figure 9 shows typical diffuse reflectance spectra for two samples. Optical transmittance measurement was not possible because of the back contact cobalt layer present in all of them. The spectra of Figure 9 have some characteristic features: structures appear in the blue-UV region superimposed to an almost smooth background. The most prominent peaks of the samples shown in Figure 9 appear at ∼370 nm (for sample prepared at

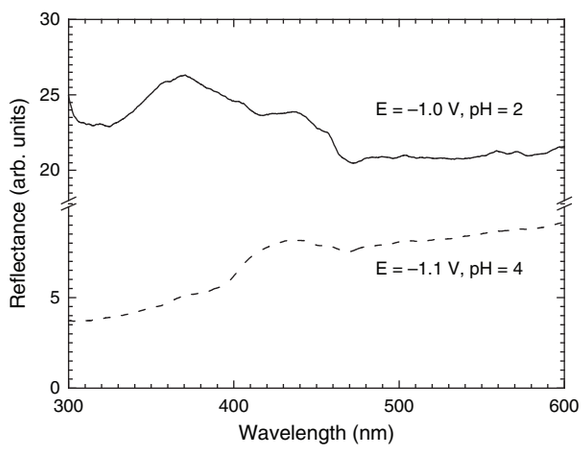

Fig. 9. Optical diffuse reflectance for two representative samples prepared at different conditions: $E = -1.0$ V and pH $= 2$ (full line) and $E = -1.1V$ and pH $= 4$ (dashed line).

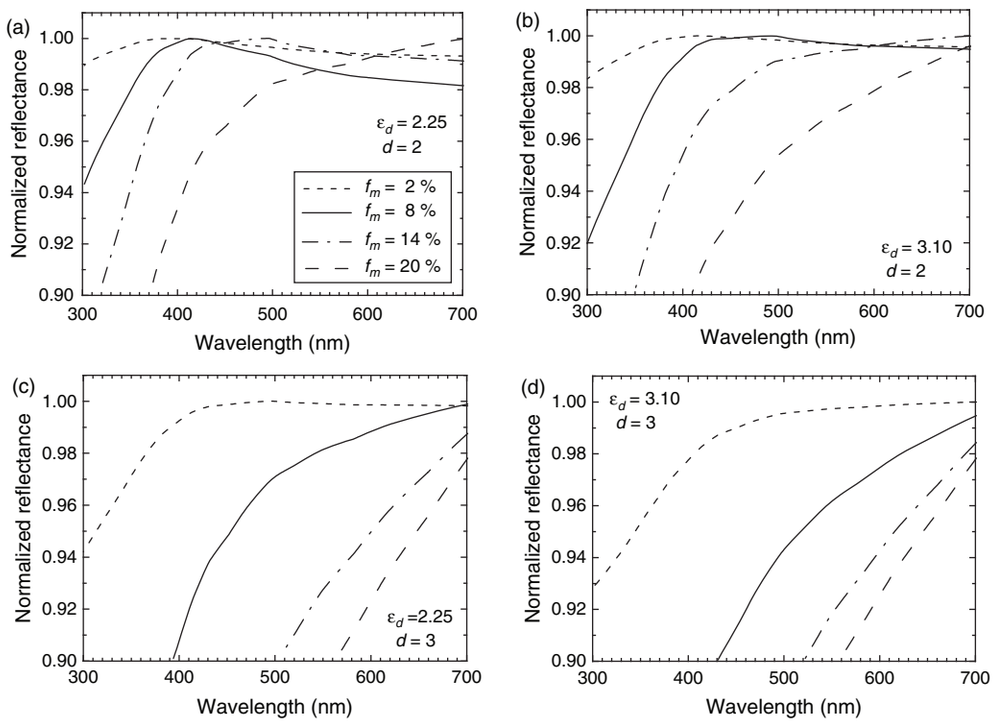

Fig. 10. Results of numerical simulation in for different cases: (a) and (b) $d = 2$, (c) and (d) $d = 3$; while $\varepsilon_d = 2.25$ for (a) and (c) and $\varepsilon_d = 3.10$ for (b) and (d). In each case for representative cases of different metal volume fractions f_m are shown: 2% (short dashed line), 8% (full line), 14% (dotted dashed line) and 20% (dashed line).

$E = -1.0$ V and pH = 2) and at ∼430 nm (for sample prepared at $E = -1.1$ V and pH = 4).

The optical properties of Co nanowires in different liquid solutions (water, ethanol, and methanol) have been previously studied.[47] In these cases an absorption peak appears at wavelength lower than 300 nm, which is interpreted as transverse surface plasmon according to the Gans theory.[63] As the cobalt nanowire under study are immersed in a dielectric template, the spectral position of this resonance strongly depend on the template dielectric constant, ε_d. For dielectric constant higher than the previous mentioned liquid solutions, it is expected that the corresponding resonance peak would shift into the visible region. However, a quantitative account with Gans theory does not allow interpreting the observed peaks in Figure 9. For this reason a model based on effective medium theory was used for a proper interpretation of the present experimental result. The model is similar to the one previously used to understand optical properties of Ag nanowires in porous alumina template[32, 64] and Ni–dielectric nanostructures.[65] In this model the reflectance is calculated as in Ref. [66], with Fresnel coefficients calculated by the usual relations.[66–68] Experimental data from the literature was used.[60, 70] The complex dielectric constant of the composite material, is calculated by Bruggeman's effective medium approximation.[64, 65, 71] The latter has been proved useful for the unfilled porous alumina template[72] and can be applied to the present samples morphology: Co nanowires in a dielectric matrix. The parameters needed in this approximation are the metal volume fraction (f_m), the dimensionality (d) of the system under consideration ($d = 3$ for spherical inclusions, while $d = 2$ for the cylindrical symmetry of the present case) and the dielectric constant (ε_d) of the alumina.[63, 71, 73]

Figure 10 shows the results of the numerical simulations for different relevant values of the parameters. Figures 10(a and b) are for a dimensionality $d = 2$ while Figures 10(c and d) are for $d = 3$. Different values for the alumina dielectric constant ε_d were used: Tabulated data for crystalline Al_2O_3 for Figures 10(b and d),[74] and reported data for porous alumina obtained by aluminum anodization for Figures 10(a and c).[71] In each case curves are shown for representative values of the metal volume fraction f_m. Results that have more resemblance with the experimental data of Figure 9 are those shown in Figure 10(a) ($\varepsilon_d = 2.25$, $d = 2$) for the curves corresponding to the lower metal filling fraction. In these cases, a peak in the reflectance appears at ∼380 nm (for $f_m \sim 2\%$) which shifts to the red as f_m increases, reaching ∼500 nm (for $f_m \sim 14\%$). For high f_m (∼20%) the curves have a smooth shape with no peak at all in the visible region. The peak is also present in the case of Figure 10(b) ($\varepsilon_d = 3.10$, $d = 3$) for low f_m, shifting also to the red as f_m increases, however it disappears at a value higher than $f_m \sim 14\%$. Notwithstanding, in the case of Figure 10(b), the curves are smoother and the structure assignable to the peak less

prominent than in Figure 10(a). Independently of the ε_d values, there is no peak present for the curves with $d = 3$, Figures 10(c and d), (except in the case of $\varepsilon_d = 2.25$ and $f_m = 2\%$ where the curve is almost flat).

A first conclusion that can be extracted is that the peaks observed for the experimental optical characterization are a structure due to the morphology of the metal-dielectric composite. Effectively, the fact that the peaks only appears in the numerical result for the case where $d = 2$, which corresponds to a two-dimensional system, is compatible with the morphology of the samples consisting in almost parallel cylindrical nanowires with their axes perpendicular to the surface substrate. Moreover, the case of Figure 10(a) corresponds also with an intermediate value for the dielectric constant of the porous alumina $\varepsilon_d = 2.25$. This value, obtained from experimental determinations of the optical properties of the porous alumina,[72] is closer to the values that would correspond to the liquid dielectric media in which optical properties of Co nanowires were previously studied.[47] Finally, the difference in spectral shape of the reflectance for different samples (as observed in Fig. 9) and the exact position of the peak, can be assigned to different metal volume fractions as consequence of the preparation conditions. A comparison of the theoretical results of Figure 10(a) with the experimental measurements of Figure 9 allows to assign a higher filling fraction to the sample prepared at $E = -1.0$ V and pH = 2 than the one prepared at $E = -1.1$ V and pH = 4. In spite of the change in structure with pH, this is consistent with the observation that there is an increase in crystallinity with electrodeposition potential (compare with Figs. 3(a) and 4(b)). Therefore the observed optical properties are a direct consequence of the morphology of the samples and there is a correlation with their cristallinity.

3.6. Magnetic Properties

Magnetic measurements have been performed in arrays of nanowires that are inmersed in the pores of the AAO membrane, so that the order and the distance between nanowires are kept constant. Figure 11 shows the hysteresis curves with the external field H, parallel ($H||$) and perpendicular ($H\perp$) to the nanowire axis, for a sample with length of $L = 4$ μm, at room temperature. For this sample the coercivity measured with the external field along and perpendicular to the axis of the nanowires changes from $H_c^{\parallel} = 770$ Oe to $H_c^{\perp} = 150$ Oe respectively. The difference between the parallel and perpendicular hysteresis curves defines the uniaxial anisotropy; the coercivity and remanence in the parallel configuration are larger than in the perpendicular configuration, indicating that the magnetic easy axis lies along the nanowire axis. Thus, the magnetic properties presented in this work are very suitable for applications in information storage media.[74, 75] The magnetic behavior of magnetic nanowire arrays is

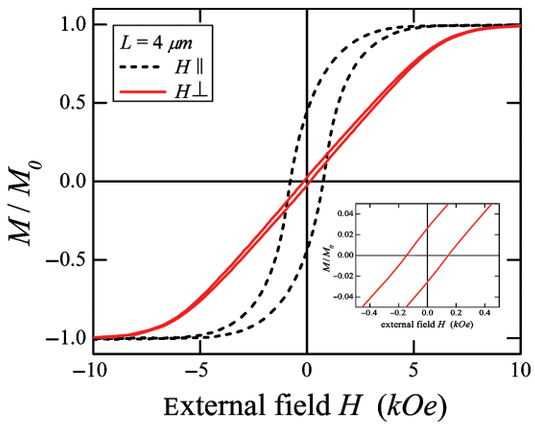

Fig. 11. Hysteresis curves with the external magnetic field parallel (H ||) and perpendicular ($H\perp$) to the nanowire axis, for a nanowires array with a nanowire length of 4 μm, 50 nm diameter, 100 nm interpore distance, $E = -0.9$ V, and pH = 2. The inset shows the amplification of the perpendicular hysteresis curves.

strongly dependent on the magnetic anisotropies (mainly the shape and crystalline anisotropy) and the dipolar interaction between nanowires. In longer nanowires, the strong shape anisotropy will induce a magnetic easy direction parallel to the nanowire axis, as can be observed in Figure 11.

We have also investigated the effect of the electrodeposition potential, E, and pH on the magnetic properties of the samples. Figure 12 shows the influence of pH at the electrodeposition potentials of (a) −0.9 V and (b) −1.1 V. For the sample fabricated at $E = -0.9$ V the coercivity measured at the pH 2 and 4 changes from to 770 to 650 Oe, and the squareness (M_r/M_0) changes from 0.44 and 0.15 respectively. For the sample fabricated at $E = -1.1$ V the coercivity measured at pH 2 and 4 changes from to 690 to 575 Oe, and the squareness changes from 0.28 and 0.21 respectively. Hence it is evident that a change in pH leads to different magnetic anisotropies on the samples, due to the dependence of crystal structures on pH (see Figs. (3 and 4)). Figure 13(a) shows the influence of the electrodeposition potential for electrolytic bath pH of 2.0. The coercivity measured at the $E = -0.9$ and -1.1 V changes from to 780 to 570 Oe, and the squareness changes from 0.44 to 0.22 respectively. Therefore, due to the dependence of the crystallinity as a function of potential, the crystalline anisotropy is also affected by electrodeposition potential (Fig. 3). Figure 13(b) shows the influence of the electrodeposition potential for an electrolytic bath pH of 4.0. In this case the coercivity measured at the $E = -0.9$ and -1.1 V changes from to 660 to 580 Oe, and the squareness changes from 0.22 to 0.15 respectively. From the above mentioned results one can infer that the different electrodeposition potentials lead to different magnetic anisotropies, due to the different crystal structures, in correspondence with Figure 4. Figure 14 summarizes the influence of the electrodeposition conditions on the coercivity and squareness for these samples.

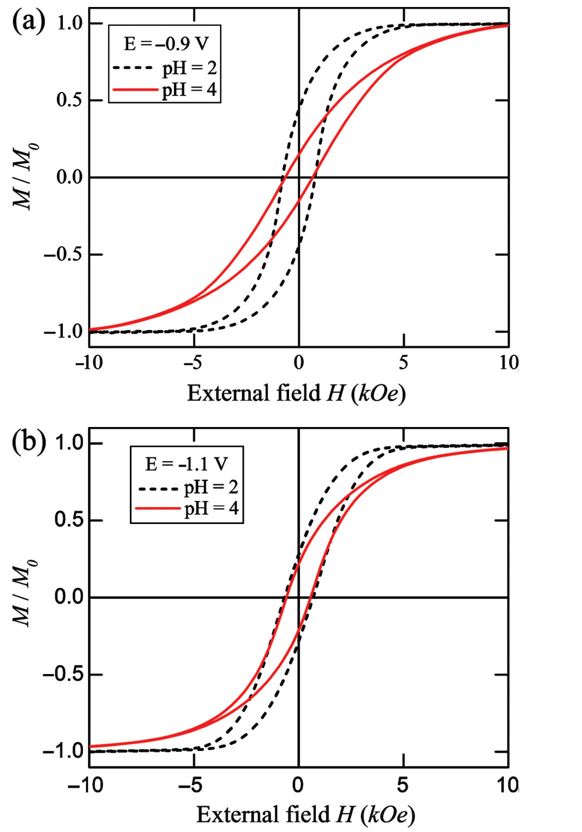

Fig. 12. Hysteresis loops of Co nanowire arrays embedded in the home made AAO template in function of the electrolytic bath pH, for two electrodeposition potentials V: (a) −0.9 v and (b) −1.0 v. All samples have the same geometric parameters ($L = 4$ μm, 50 nm diameter, and 100 nm interpore distance). The external magnetic field is applied parallel to the nanowire axis.

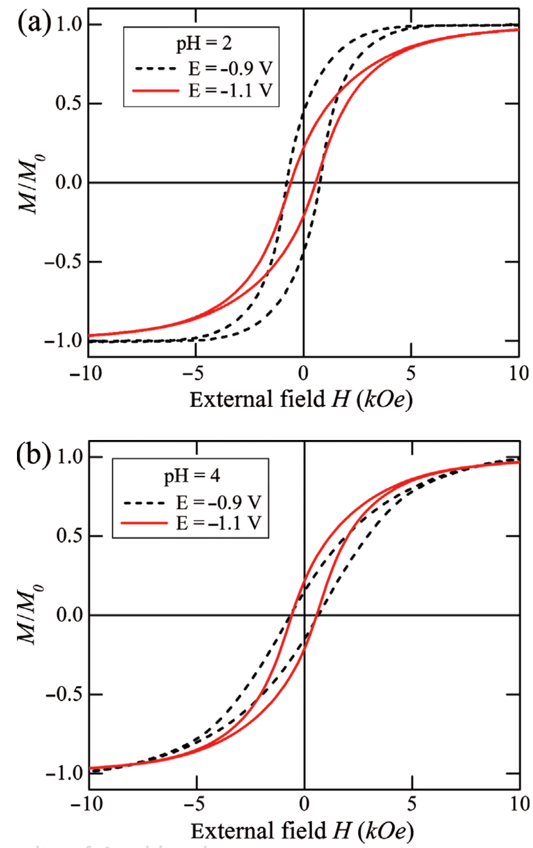

Fig. 13. Hysteresis loops of Co nanowire arrays embedded in the home made AAO template in function of the electrodeposition potentials, for two electrolytic bath pH: (a) 2 and (b) 4. All samples have the same geometric parameters ($L = 4$ μm, 50 nm diameter, and 100 nm interpore distance). The external magnetic field is applied parallel to the nanowire axis.

The effective magnetic anisotropy of the nanowire arrays is determined by four contributions:

(i) the shape anisotropy, which will induce a magnetic easy axis parallel to the nanowire axis,

(ii) the dipolar interaction between nanowires, which will induce a magnetic easy axis perpendicular to the nanowire axis,

(iii) the crystalline anisotropy and

(iv) the magnetoelastic anisotropy, due to stress between the template and the nanowires, that induce a magnetic easy axis parallel or perpendicular to the stress direction. In Co nanowires the contribution of the magnetoelastic anisotropy at ambient temperature is negligible compared to other anisotropies terms.[76,77] Thus, the effective anisotropic field of a Co nanowire array is

$$H_k = 2\pi M_0 - 6.3\pi M_0 r^2 L/D^3 + H_{\text{cris}} \qquad (6)$$

where M_0 is the saturation field, r is the radius of nanowires, D is the separation between nanowires, and L is the nanowire length.[78] The first term in Eq. (9) is the shape anisotropy field, the second term is the dipolar field acting on one nanowire due to all other nanowires in the array, and the third term is the crystalline anisotropy field that is dependent on the growth conditions of the nanowires (electrodeposition conditions). This expression predicts that H_k depends directly of the crystalline anisotropy as our experimental results demonstrate. Changes in the coercivity and remanence due to contribution of the crystalline anisotropy

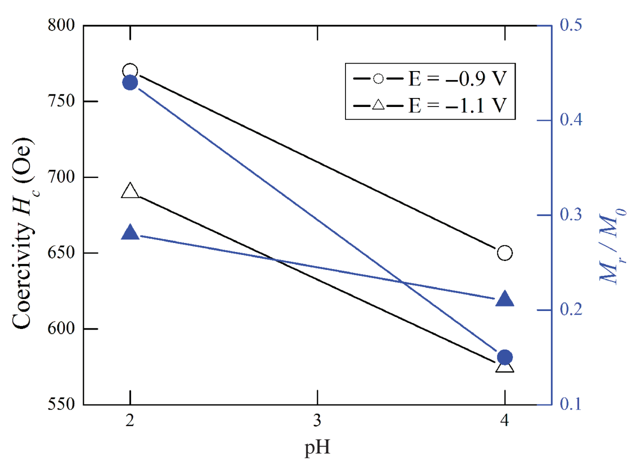

Fig. 14. Coercivity and squarennes in function of: pH and electrodeposition potential E, corresponding to Figures 12 and 13, respectively.

are usually small since the shape anisotropy and dipolar interaction between nanowires are predominant, as predicted by Eq. (9).

4. CONCLUSIONS

Cobalt nanowires with controllable orientation and phase structure have successfully been grown by the potentiostatic electrodeposition technique within the pores of AAO templates. It has been found that the proper selection of the deposition potential and pH value is very important in controlling the crystallographic orientation and phase structure of the cobalt nanowires. Cobalt nanowires with hcp and fcc phase structure have been prepared. At pH = 4 and at −1.1 V (vs. Ag/AgCl) single crystalline nanowires with a hcp phase with a strong (20$\bar{2}$1) orientation, so far not reported, were obtained. High temperatures contributed to improve the single crystalline character of the cobalt nanowires. The presence of chloride anion in the electrolytic bath has also a very important influence on the structural properties of the resulting cobalt nanowires, improving their crystallinity. The obtained nanowires have average diameters of 50 nm and lengths of 6 μm which is equivalent to the pore size and thickness of the AAO membranes. The optical properties reveal a peak in the reflectance between 370 nm and 430 nm. These structures can be interpreted by a numerical simulation that account for the properties of the composite material by means of Bruggeman's effective medium approximation. The results of these simulations allow to assign the peaks to the two dimensional morphology of the samples consisting in almost parallel cylindrical nanowires with it axes perpendicular to the substrate surface. Finally, in Co nanowire array samples the magnetic anisotropy is dependent of the electrodeposition potential and the electrolytic bath pH. Therefore, the magnetic properties of interest (coercivity and remanence) can be adjusted by controlling the pH and potential.

Acknowledgments: This work has been supported by FONDECYT (Chile) project 3080058, 3100117, and 1080164. The financial support of CENAVA project PBCT-ACT027 is also acknowledged. Ricardo E. Marotti and Enrique A. Dalchiele thank to CSIC (Universidad de la República), and to PEDECIBA-FISICA (Uruguay). Ricardo E. Marotti also acknowledges ANII. The authors thank J. Troccoli and A. Marquez for SEM measurements.

References and Notes

1. C. L. Chien, L. Sun, M. Tanase, L. A. Bauer, A. Hultgren, D. M. Silevitch, G. J. Meyer, P. C. Searson, and D. H. Reich, *J. Magn. Magn. Mat.* 249, 146 (**2002**).
2. M. Hernández-Vélez, *Thin Solid Films* 495, 51 (**2006**).
3. H. He and N. J. Tao, Encyclopedia of Nanoscience and Nanotechnology, edited by H. S. Nalwa, American Scientifi Publishers, Los Angeles, CA, (**2003**), Vol. 10, pp. 1–18.
4. M. Kröll, W. J. Blau, D. Grandjean, R. E. Benfield, F. Luis, P. M. Paulus, and L. J. de Jongh, *J. Magn. Magn. Mater.* 249, 241 (**2002**).
5. J.-L. Maurice, D. Imhoff, P. Etienne, O. Durand, S. Dubois, L. Piraux, J. -M. George, P. Galtier, and A. Fert, *J. Magn. Magn. Mater.* 184, 1 (**1998**).
6. J. I. Martín, J. Nogués, K. Liu, J. L. Vicent, and I. K. Schuller, *J. Magn. Magn. Mater.* 256, 449 (**2003**).
7. A. Fert and L. Piraux, *J. Magn. Magn. Mater.* 200, 338 (**1999**).
8. S. Karmakar, P. K. Tyagi, D. S. Misra, and S. M. Sharma, *Phys. Rev. B.* 73, 184119 (**2006**).
9. Y. J. Kang, J. Choi, C.-Y. Moon, and K. J. Chang, *Phys. Rev. B* 71, 115441 (**2005**).
10. J. Xu and Y. Xu, *Mater. Lett.* 60, 2069 (**2006**).
11. K. R. Pirota, D. Navas, M. Hernández-Vélez, K. Nielsch, and M. Vázquez, *J. Alloys and Compd.* 369, 18 (**2004**).
12. X. Huang, L. Li, X. Luo, X. Zhu, and G. Li, *J. Phys. Chem. C* 112, 1468 (**2008**).
13. A. Krause, M. Uhlemann, A. Gebert, and L. Schultz, *Thin Solid Films* 515, 1694 (**2006**), and references therein.
14. M. Darques, L. Piraux, A. Encinas, P. Bayle-Guillemaud, A. Popa, and U. Ebels, *Appl. Phys. Lett.* 86, 072508 (**2005**).
15. G. Kartopu, O. Yalçin, M. Es-Souni, and A. C, Başaran, *J. Appl. Phys.* 103, 093915 (**2008**).
16. M. Lai and D. Jason Riley, *Coll. Inter. Sci.* 323, 203 (**2008**).
17. A. Huczko, *Appl. Phys. A* 70, 365 (**2000**).
18. T. R. Kline, M. Tian, J. Wang, A. Sen, M. W. H. Chan, and T. E. Mallouk, *Inorg. Chem.* 45, 7555 (**2006**).
19. V. M. Prida, K. R. Pirota, D. Navas, A. Asenjo, M. Hernández-Vélez, and M. Vázquez, *Nanosci. Nanotechnol.* 7, 272 (**2007**).
20. M. C. Kum, B. Y. Yoo, Y. W. Rheem, K. N. Bozhilov, W. Chen, A. Mulchandani, and N. V. Myung, *Nanotechnology* 19, 325711 (**2008**).
21. I. U. Schuchert, M. E. Toimil Molares, D. Dobrev, J. Vetter, R. Neumann, and M. Martin, *J. Electrochem. Soc.* 150, C189 (**2003**).
22. H. Masuda and K. Fukuda, *Science* 268, 1466 (**1995**).
23. O. Jessensky, F. Müller, and U. Gösele, *J. Electrochem. Soc.* 145, 3735 (**1998**).
24. S. Ono, M. Saito, M. Ishiguro, and H. Asoh, *J. Electrochem. Soc.* 151, B473 (**2004**).
25. K. Nielsch, J. Choi, K. Schwirn, R. B. Wehrspohn, and U. Gösele, *Nano Lett.* 2, 677 (**2002**).
26. J. Verbeeck, O. I. Lebedev, G. Van Tendeloo, L. Cagnon, C. Bougerol, and G. Tourillon, *J. Electrochem. Soc.* 150, E468 (**2003**).
27. A. Cortés, G. Riveros, J. L. Palma, J. C. Denardin, R. E. Marotti, E. A. Dalchiele, and H. Gómez, *Nanosci. Nanotechnol.* 9, 3 1992 (**2009**).
28. M. Tian, J. Wang, J. Kurtz, T. E. Mallouk, and M. H. W. Chan, *Nano Lett.* 3, 919 (**2003**).
29. G. Riveros, H. Gómez, A. Cortés, R. E. Marotti, and E. A. Dalchiele, *Appl. Phys. A* 81, 17 (**2005**).
30. G. Riveros, H. Gómez, R. Schrebler, R. E. Marotti, and E. A. Dalchiele, *Electrochem. Solid-State Lett.* 11, K19 (**2008**).
31. G. Riveros, S. Green, A. Cortés, H. Gómez, R. E. Marotti, and E. A. Dalchiele, *Nanotech.* 17, 561 (**2006**).
32. E. A. Dalchiele, R. E. Marotti, A. Cortés, G. Riveros, H. Gómez, L. Martínez, R. Romero, D. Leinen, F. Martín, and J. R. Ramos-Barrado, *Physica E: Low-dimensional Systems and Nanostructures* 37, 184 (**2007**).
33. F. Maurer, J. Brötz, S. Karim, M. E. Toimil Molares, C. Trautmann, and H. Fuess, *Nanotechnology* 18, 135709 (**2007**).
34. X. W. Wang, G. T. Fei, P. Tong, X. J. Xu, and L. D. Zhang, *J. Cryst. Growth* 300, 421 (**2007**).
35. H. Pan, B. Liu, J. Yi, C. Poh, S. Lim, J. Ding, Y. Feng, C. H. A. Huan, and J. Lin, *J. Phys. Chem. B* 109, 3094 (**2005**).
36. M. A. Kashi, A. Ramazani, and A. Khayyatian, *J. Phys. D: Appl. Phys.* 39, 4130 (**2006**).

37. F. Li, T. Wang, L. Ren, and J. Sun, *J. Phys.: Condens. Matter* 16, 8053 **(2004)**.
38. P. Wang, L. Gao, Z. Qiu, X. Song, L. Wang, S. Yang, and R. Murakami, *J. Appl. Phys.* 104, 064304 **(2008)**.
39. J. Zhang, G. A. Jones, T. H. Shen, S. E. Donnelly, and G. Li, *J. Appl. Phys.* 101, 054310 **(2007)**.
40. Y. Peng, T.-H Shen, and B. Ashworth, *J. Appl. Phys.* 93, 7050 **(2003)**.
41. M. Gilliot, A. E. Naciri, L. Johann, J. P. Stoquert, J. J. Grob, and D. Muller, *J. Appl. Phys.* 101, 014319 **(2007)**.
42. M. Gilliot, A. E. Naciri, L. Johann, J. P. Stoquert, J. J. Grob, and D. Muller, *Phys. Rev. B* 76, 045424 **(2007)**.
43. M. Gilliot, A. E. Naciri, L. Johann, J. P. Stoquert, J. J. Grob, and D. Muller, *Phys. Rev. B* 74, 045423 **(2006)**.
44. G. A. Niklasson and C. G. Granqvist, *J. Appl. Phys.* 55, 3382 **(1984)**.
45. E. Anno, *Phys. Rev. B* 50, 17502 **(1994)**.
46. A. Azarian, A. Iraji zad, and A. Dolati, *Opt. Commun.* 274, 471 **(2007)**.
47. H. Pan, W. Chen, Y. P. Feng, W. Ji, and J. Lin, *Appl. Phys. Lett.* 88, 223106 **(2006)**.
48. H. J. Tang, F. Q. Wu, and S. Zhang, *Appl. Phys. A* 85, 29 **(2006)**.
49. T. Cohen-Hyams, W. D. Kaplan, and J. Yahalom, *Electrochem. Solid State Lett.* 5, C75 **(2002)**.
50. S. Nakahara and S. Mahajan, *J. Electrochem. Soc.* 127, 283 **(1980)**.
51. B. D. Cullity, Elements of X-ray Diffraction, 2nd. edn., Addison Wesley, Reading, MA **(1978)**.
52. M. T. Wu, I. C. Leu, J. H. Yen, and M. H. Hon, *J. Phys. Chem. B* 109, 9575 **(2005)**.
53. H. Pan, H. Sun, C. Poh, Y. Feng, and J. Lin, *Nanotechnology* 16, 1559 **(2005)**.
54. X. W. Wang, G. T. Fei, X. J. Xu, Z. Jin, and L. D. Zhang, *J. Phys. Chem. B* 109, 24326 **(2005)**.
55. H. Sun, X. Li, Y. Chen, W. Li, F. Li, B. Liu, X. Zhang, *Nanotechnology* 19, 225601 **(2008)**.
56. J. T. Matsushima, F. Trivinho-Strixino, and E. C. Pereira, *Electrochem. Acta* 51, 1960 **(2006)**.
57. H. Nakano, K. Nakahara, S. Kawano, S. Oue, T. Akiyama, and H. Fukushima, *J. Appl. Electrochem.* 32, 43 **(2002)**.
58. N. A. Pangarov, *J. Electroanal. Chem.* 9, 70 **(1965)**.
59. T. C. Franklin, *Surf. Coat. Technol.* 30, 415 **(1987)**.
60. L. Hu and G. Chen, *Nano Lett.* 7, 3249 **(2007)**.
61. R. A. Street, P. Qi, R. Lujan, and W. S. Wong, *Appl. Phys. Lett.* 93, 163109 **(2008)**.
62. C. F. Bohren and D. R. Huffman, Absorption and Scattering of Light by Small Particles, John Wiley & Sons, New York **(1983)**.
63. S. Green, A. Cortés , G. Riveros, H. Gómez, E. A. Dalchiele, and R. E. Marotti, *Phys. Stat. Sol. (c)* 4, 340 **(2007)**.
64. P. A. Galione, A. L. Baroni, J. R. Ramos-Barrado, D. Leinen, F. Martín, R. E. Marotti and E. A. Dalchiele, *Surface Coatings Technol.* 204, 2197 **(2010)**.
65. D. G. W. Goad and M. Moskovits, *J. Appl. Phys.* 49, 2929 **(1978)**.
66. J. D. Jackson, Classical Electrodynamics, 3rd edn., Wiley, New York **(1998)**.
67. P. Y. Yu and M. Cardona, Fundamentals of Semiconductors, 2nd edn., Springer-Verlag, Berlin **(1999)**.
68. P. B. Johnson and R. W. Christy, *Phys. Rev. B* 6, 4370 **(1972)**.
69. P. B. Johnson and R. W. Christy, *Phys. Rev. B* 9, 5056 **(1974)**.
70. D. E. Aspnes, *Am. J. Phys.* 50, 704 **(1982)**.
71. A. C. Gâlcã, E. S. Kooij, H. Wormeester, C. Salm, V. Leca, J. H. Rector, and B. Poelsema, *J. Appl. Phys.* 94, 4296 **(2003)**.
72. O. Stenzel, The Physics of Thin Film Optical Spectra: An Introduction, Springer, Berlin **(2005)**.
73. W. J. Tropf, M. E. Thomas, and T. J. Harris, Properties of Crystals and Glasses, edited by M. Bass, E. W. Van Stryland, D. R. Williams, and W. L. Wolfe, Handbook of Optics, Mc Graw Hill Inc., New York **(1996)**, Vol. 2, Chap. 33.
74. K. Nielsch, R. B. Wehrspohn, J. Barthel, J. Kirschner, U. Gösele, S. F. Fischer, and H. Kronmüller, *Appl. Phys. Lett.* 79, 1360 **(2001)**.
75. K. Nielsch, R. B. Wehrspohn, J. Barthel, J. Kirschner, S. F. Fischer, H. Kronmüller, T. Schweinböck, D. Weiss, and U. Gösele, *J. Magn. Magn. Mater.* 249, 234 **(2002)**.
76. K. R. Pirota, E. L. Silva, D. Zanchet, D. Navas, M. Vázquez, M. Hernández-Vélez, and M. Knobel, *Phys. Rev. B* 76, 233410 **(2007)**.
77. E. L. Silva, W. C. Nunes, M. Knobel, J. C. Denardin, D. Zanchet, K. Pirota, D. Navas, and M. Vázquez, *Physica B* 384, 22 **(2006)**.
78. G. C. Han, B. Y. Zong, P. Luo, and Y. H. Wu, *J. Appl. Phys.* 93, 9202 **(2003)**.

Received: 6 May 2010. Accepted: 17 August 2010.